SAND2019-10294C

Operational Modes of a 2.0 MW_{th} Chloride Molten-Salt Pilot-Scale System

Kenneth M. Armijo[1], Matthew D. Carlson[2], Dwight S. Dorsey[3], Jesus D. Ortega[2], Dimitri A. Madden[2], Joshua M. Christian[2], and Craig S. Turchi[4]

[1]Ph.D., Sandia National Laboratories, P.O. Box 5800, MS-1127, Albuquerque, NM 87185-1127, (505) 284-3425, kmarmij@sandia.gov

[2]Concentrating Solar Power Department 06123, Sandia National Laboratories, PO 5800 MS 1127, Albuquerque NM, 87185, USA.

[3]Bridgers and Paxton, 4600-C Montgomery Blvd NE, Albuquerque, NM 87109, USA.

[4]National Renewable Energy Laboratory, 15013 Denver West Parkway, Golden, CO 80401, USA.

Abstract. The limit of traditional solar-salt thermal stability is around 600 °C with ambient air as the cover gas. Nitrate molten salt concentrating solar power (CSP) systems are currently deployed globally and are considered to be state-of the art heat transfer fluids (HTFs) for present day high-temperature operation. However, decomposition challenges occur with these salts for operation beyond 600 □. Although slightly higher limits may be possible with solar salt, to fully realize SunShot efficiency goals of \$15/kWh_{th} HTFs and an LCOE of 6¢/kWh, molten-salt technologies working at higher temperatures (e.g., 650 °C to 750 °C) will be require an alternative salt chemistry composition, such as chlorides. In this investigation a 2.0MWth Pilot-scale CSP plant design is developed to assess thermodynamic performance potential for operation up to 720 □. Here, an Engineering Equation Solver (EES) model is developed with respect to 14 state-points from the base of a solar tower at the Sandia National Laboratories, National Solar Thermal Test Facility (NSTTF), to solar receiver mounted 120 ft. above the ground. The system design considers a ternary chloride ternary chloride (20%NaCl/40%MgCl/40%KCl by mol%) salt as the HTF, with 6 hrs. of storage and a 1 MWth primary salt to sCO_2 heat exchanger. Preliminary system modelling results indicate a minimum *C*v of 60 required for both cold and hot-side throttle recirculation valves for the operational pump operating between speeds of 1800 and 2400 RPM. Further receiver comparison study results suggest that the ternary chloride salt required an average 11.1% lower receiver flux with a slightly lower calculated receiver efficiency when compared to a high-temperature fluoride salt for the desired receiver system design.

INTRODUCTION

Molten-salt technology using nitrate salts in tubular external receivers is the current state-of-the art CSP technology with hot-salt operational temperatures of approximately 565 °C. Currently, there are multiple commercial molten-salt solar power towers (SPT) that employ a sodium/potassium nitrate, or "solar salt," as both the heat transfer fluid (HTF) and thermal energy storage (TES) medium: Gemasolar (Spain, 19 MW_e, 15 hours TES [1]), Crescent Dunes (Tonopah, Nevada, 110 MW_e, 10 hours TES [2]), and Noor III (Ouarzazate, Morocco, 134 MW_e, 7 hours TES). Overall, interest in solar salt HTF has increased where there are presently approximately 37 existing solar power tower (SPT) projects in operation or development globally [5]. The limit of solar salt thermal stability is around 600 °C with ambient air as the cover gas. To further increase system efficiency however, next generation molten salts being considered for U.S. Department of Energy (DOE) Generation 3 systems are currently investigating a ternary 20%NaCl/40%MgCL/40%KCl chloride salt blend to facilitate CSP operation as high as 735 □ (at the receiver outlet). Subsequently, the Gen 3 Liquid-Pathway team, comprised of various research institutions, and led by the National Renewable Energy Laboratory (NREL), are developing a concentrating solar power (CSP) system to advance molten-salt systems technology from the current state of-the-art solar-salt/Steam Rankine design, embodied by industrial plants [2] operating at 565 °C and ~42% thermo-electric conversion efficiency. The project development is toward a next-generation salt or alkali metal receiver HTF capable of interfacing with a supercritical carbon dioxide (sCO_2) Brayton cycle operating at 720 °C and ~50% efficiency. A thermodynamic system model for a 2-MW_{th} molten-salt test loop has been developed with a target receiver temperature of 735 °C, with hot and cold tank temperatures of 720 °C and 500 °C respectively. The system design includes TES of 6 hours, based on an approximate 8.0 kg/s mass flow rate and 46,800-gallon salt inventory. In this investigation, engineering design has been performed for the system design of a Pilot-scale molten salt test loop to be operated at the Sandia National Laboratories National Solar Thermal Test Facility (NSTTF), where a steady operational mode was investigated for characterization of 14 thermodynamic state points and pump system curves. This result assumes ideal receiver absorption and heat transfer through the primary heat exchanger (PHX).

SYSTEM PROCESS DESIGN MODELLING

A thermodynamic system design model was developed using Engineering Equation Solver (EES) where state properties were calculated at inlets and outlets along both hot and cold legs of the pilot-scale plant. For this investigation, this model was constructed from a series of subroutines that were integrated in a top-level file to solve a closed set of equations. Models were set up together in pairs, with a component model having an odd inlet state index (i.e., 1) and set up to solve for its even outlet state index (i.e., 2) and followed by a piping model which uses the previous even outlet state as its inlet state, which then solves for its odd outlet state (i.e., 3). This simplifies tracking component and piping model results based on their inlet state index. User-supplied inputs and calculation settings are supplied through the EES diagram window and via lookup tables, as well as parametric tables as appropriate for the solution configuration. Data from any user input method can be saved to and loaded from a file to simplify scenario modeling without requiring multiple copies of the EES code itself. The EES model was developed to be configurable to facilitate parametric studies related to pump design, heat exchanger design, etc. Although several transient operational modes are presently being developed with respect to fill, drain and contingency senarios, this investigation only considers the steady operation of the system during the final attemporation mode as shown in Fig. 1. This system was modelled with flow from the cold tank (maintained at 500 □) at the base of SPT (inset picture), up a riser test section to a 2.0 MW_{th} reciever section at the 120 ft. level of the NSTTF solar tower. The salt is then expected to exist the reciever at a temperature of 730 □, and flow down a downcomer hot leg to a hot salt tank, operated at 720 □. The salt then flows to a primary heat exchanger which transfers up to 1 MW_{th} of heat to an sCO_2 loop (not discussed here) with a designed salt-side mass flow rate of 4.4 kg/s. The salt then flows back at a lower 500 □ temperature to the cold tank, where it is flows in through a sparger to help with thermal-fluid mixing. Recirculation is expected to occur for both the cold and hot tank systems using respective recirculation valves. Various approximations are made with this simplified process diagram, such as the exclusion of an attemporation pump, salt chemistry provisions and ulage gas system source equipment and additional salt heat mixing tanks.

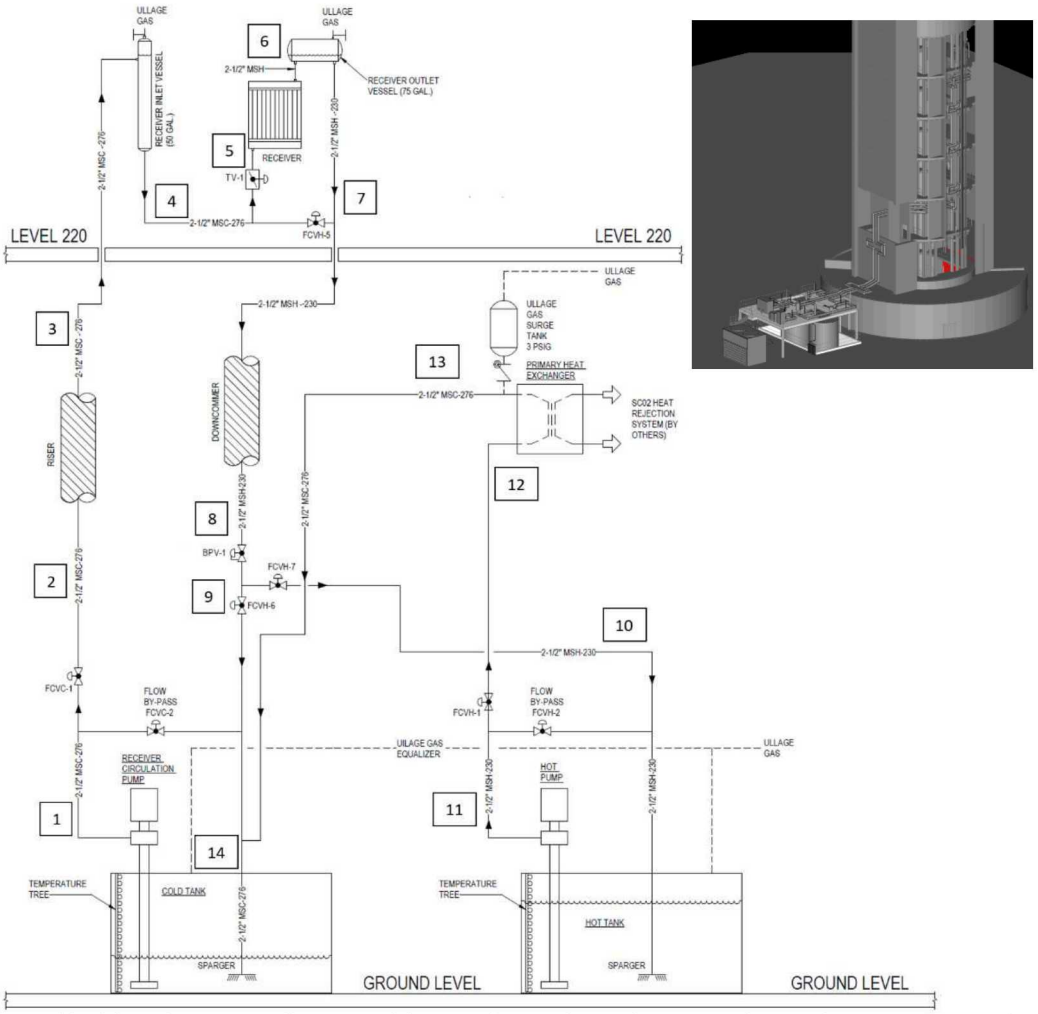

Figure 1. Molten chloride salt process diagram with EES thermodynamic state points and 3D system Revit model design (inset figure).

The system modeling framework that was built within the Engineering Equation Solver (EES) computational model consists of a number of reusable components that model processes between states in the system, including models pertaining to the tank, pumps, thermal transport piping, valves, primary salt/sCO_2 heat exchanger, and receiver. These models, also built within EES, can be reused multiple times in the system and upgraded to include the necessary complexity for any given simulation problem. Some models, including that for the tank, may incorporate transient effects requiring steady state approximations, while others such as the pump model, assume quasi-steady state conditions as any transient effects are assumed negligible at the systems-level compared to those of other components. For this investigation comparison studies were performed to assess impacts related to total dynamic head (TDH) and pressure drops across major components such as the receiver, PHX, downcomer and riser. The TDH values were used for sizing of respective system and pump operational curves. The total length of piping used in the system is tentatively calculated to be 833 ft (254 m) with a 2.5-inch schedule 80 (2.323-inch inner diameter), Haynes 230 nickle-based alloy for the hot leg, and a stainless steel c-276 alloy for the cold leg. Heat losses along the respective flow-legs will be evaluated with respect to total system efficiency. A ternary flouride salt (26%LiF/37%NaF/37%ZrF_4) was selected for this investigation, and was considered as a comparison salt based on its thermophysical properties, such as its melting point which is similar to the chloride salt, though with a value of 436 □ [7]. where sodium chloride is added to create the ternary (20%NaCl/40%MgCl/40%KCl) chloride salt [6] being employed in the current DOE Gen 3 Liquid-Pathway project. This ternary chloride salt was selected due to its lower melting point, higher heat capacity, and lower cost than other high-temperature salt chemistries, where other salts have been shown to be too expensive, unstable, or have substantial vapor pressure challenges [4].

The receiver sub-model, Fig. 2, is was developed to accept a uniform heat flux and assess heating along vertical receiver tubes over a steady basis. Future development however will later consider accepting SolTrace incident beam information from the SNL NSTTF Heliostat field with transient contributions and flux distributions in two dimensions. The thermal model includes loses from the receiver tubes due to convection and radiation where further input in a later study will be used to update the geometry and materials.

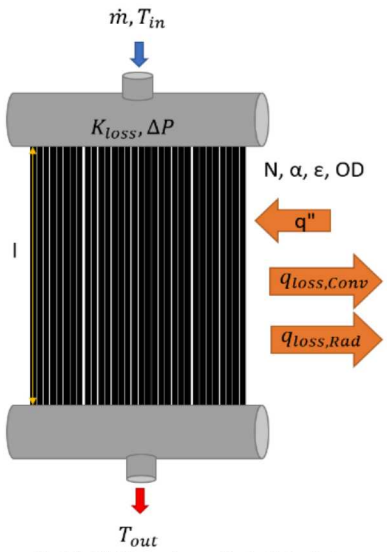

Figure 2. EES Receiver Sub-Model.

The receiver model considers a panel with N number of tubes to allow a mass flow rate and a pressure drop. It also considers in addition to uniform heat flux, uniform flow through the tubes Eqns. 1-3, with grey properties approximated for the tubes:

$$q_{abs,tube} = \frac{\alpha q_{in}}{N} \tag{1}$$

$$q_{loss} = h_{\infty}\left(T_{s,OD} - T_{\infty}\right) + \varepsilon\sigma\left(T_{s,OD}^4 - T_{\infty}^4\right) \tag{2}$$

$$Q_c = \frac{2\pi Lk}{\ln\left({}^{OD}/_{ID}\right)}\left(T_{s,OD} - T_{s,ID}\right) \tag{3}$$

where: $q_{abs,fld} = h_{ms}\left(T_{s,OD} - T_b\right)$, $q_{abs,fld} = \dot{m}C_p(T_{out} - T_{in})$, h_{ms} (Forced Internal Convection), and h_{∞} (natural external convection). In addition, the following flow equations have also been incorporated into the model to assess pressure drop across the receiver.

$$\dot{m} = N\rho A_c U \tag{4}$$

$$\Delta P = \left(f\frac{L}{ID} - \sum K\right)\frac{\rho U^2}{2} \tag{5}$$

$$\frac{1}{\sqrt{f}} = -2.0\log\left(\frac{\epsilon/_{ID}}{3.7} + \frac{2.51}{Re\sqrt{f}}\right) \text{(iterate)} \tag{6}$$

$$Re = \frac{\rho\, U\, ID}{\mu} \tag{7}$$

The tank submodel, with a general depiction shown in Figure 3, assumes a perfectly insulated, constant cross-section tank containing a homogeneous liquid covered by a non-pressurized head of gas. This configuration is an approximate representation of a well-insulated tank with a well-mixed liquid and an ullage gas system that maintains a constant 5 psi gas pressure for the tank salt inventory.

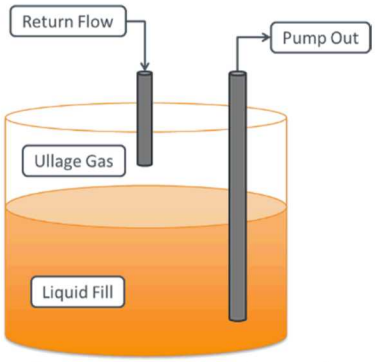

Figure 3. A schematic of the transient tank model in EES.

Differential equations were derived using control volume formulations for conservation of mass and conservation of energy pertaining to the volume of liquid in the tank. Eqns. 8 and 9 were derived to track the time rate of volume change and temperature within the liquid control volume, neglecting any effects of kinetic or potential energy as the flow velocities and differences in elevation within the liquid are negligible compared to the effects of varying inventory and temperature. The properties of the liquid are further treated as quasi-steady state, meaning that the partial derivatives of the density, specific internal energy, and specific heat capacity with respect to time (or equivalently temperature and pressure) are assumed negligible. Instead, the effect of temperature on these properties is incorporated by recalculating them at each new time step using the temperature and the previous time step.

$$\frac{dV}{dt} = \frac{\rho_{in}}{\rho}\dot{V}_{in} - \dot{V}_{out} \tag{8}$$

$$\frac{dT}{dt} = \frac{\dot{q}_{in} + h_{in}\rho_{in}\dot{V}_{in} - h\rho\dot{V}_{out} - u\rho(dV/dt)}{V\rho c_v} \tag{9}$$

The pump model was implemented as a standard quadratic head rise formula with fitting coefficients derived from actual head-flow curves, with estimations based on design requirements for a desired head-flow curve. Scaling laws for the pumps were used to convert the quadratic head rise formula derived for a single reference speed to other speeds in order to capture the effects of a variable speed drive on the pump. This model assumes the pump can start-up and vary speed rapidly enough that transient effects are negligible, and further neglects any transient effects from filling or heat transfer as negligible compared to those from the tanks, receiver, heat exchanger, and piping. Performance coefficients were fit to the head-flow data at the design speed, where head rise at lower speeds was calculated.

The thermal transport piping model currently uses a zero-dimensional thermal resistance network model to address heat transfer effects in the piping. This model captures effects from internal convection, conduction through the pipe wall, trace heating shell, insulation, and mixed external convection to the ambient air maintained at along with a variable trace heating value. The model can be solved implicitly if trace heating values are set directly but is more conveniently solved explicitly by assuming a perfectly-controlled trace heating system that ensures isothermal flow within the piping. In this way the required trace heating power can be determined even under transient conditions.

The valve model, like the pump model also assumes steady-state liquid flow behavior and neglects any transient effects or effects from heat transfer as negligible compared to other components in the system. The flow rate

through the valve is calculated using the ISA S75.01 equation for sizing control valves. The C_v value can then be varied either linearly with the valve opening percentage or based on nominal C_v curves for the type of valve to simulate off-design conditions. Note that this equation must be used carefully with an appropriate C_v based off flow in gpm and differential pressure in psid to avoid the use of extra coefficients to convert units.

The heat exchanger model uses the sub-heat exchanger method from Nellis and Klein [5] to represent a single counter-flow heat exchanger using a series of sub-heat exchangers in order to capture the effects of varying fluid properties. Although property variations in the primary heat exchanger will be minimal, this generalized model can be used for any combination of heat exchanger fluids with either side being hot or cold.

RESULTS & DISCUSSION

A parametric analysis was performed for a simple tubular receiver with a single-pass design. Required receiver flux and receiver efficiencies were calculated for an estimated 2.56 m^2 aperture area based on SolTrace studies, performed with the NSTTF heliostat field and the 120 ft. test section of the solar tower. This model was developed employing 40 single-pass tubes that were 0.5 NPS Sch. 10, constructed of an H230 material. The emissivity of the receiver was set to 0.9 where it had an assumed relative roughness of 6.42×10^{-4}. An assessment was performed to compare receiver performance between three molten salt chemistries that can operate up to 735 □ where the required flux was calculated with respect to tube diameter and thermal convection losses.

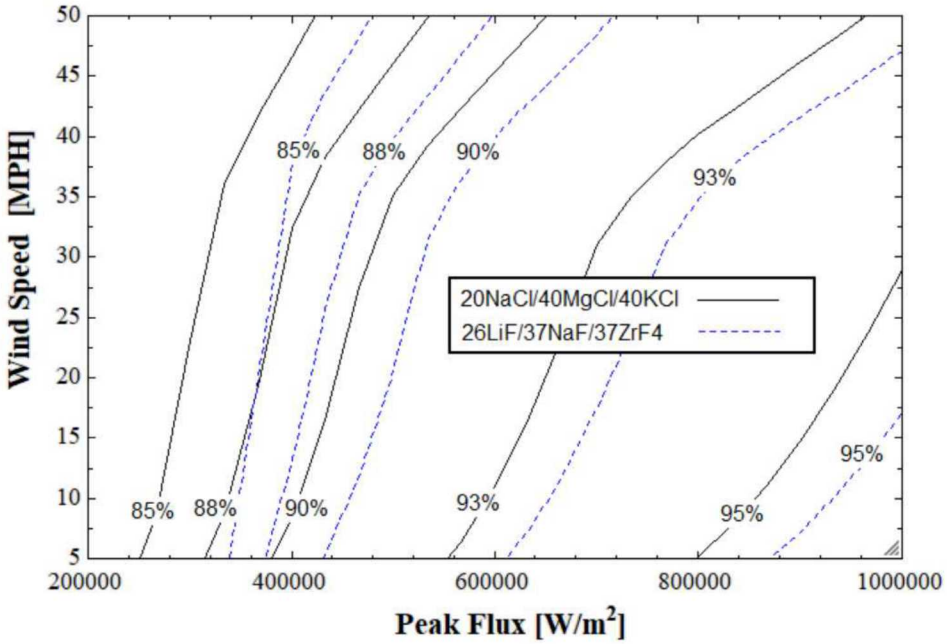

Figure 4. Receiver efficiencies as a function of required peak flux and wind speed for a chloride and flouride molten salt, considering a 500 □ and 735 □ inlet and outlet temperature and a 2.56 m^2 aperature area.

The results from Fig. 4 indicate that as the peak flux of the receiver increases for a uniform flux distribution and tube geometry, reciever efficiency sensitivity due to wind also increases. With respecct to convection losses due to wind, required peak flux for the ternary chloride salt was found to increase with wind speed by 33.3% for an 85% receiver efficiency, and 21.7% for a 95% receiver efficiency from a wind speed of 5 to 50 mph. For the flouride salt, the required peak flux levels were found to be an higher by an overal average of 11.1%, though the sensitivities were found to be less for receiver efficiencies less than 90%, and greater for receiver eficiencies greater than 93%, where for a 95% receiver efficiency, the peak flux was found to increase by 13.7% for a wind speed from 5 to 17 mph.

Further analysis was performed assessing receiver efficiencies as a function of tube diameter and convection losses based on wind speed. As shown in Fig. 5 receiver efficiency was found to be overall higher for the ternary flouride salt by an average of 1.2% than the ternary chloride salt. This could primarily be due to the higher thermal conductivity of the flouride salt, which for a temperature of 735 □ was found to be 0.59 W/m-K versus that of the chloride salt which was approximately 0.4. Additionally, the results suggest little difference between the two salts for varying tube diameters where variation between 0.5 in. to 3 in. only found an increase of approximately 2%.

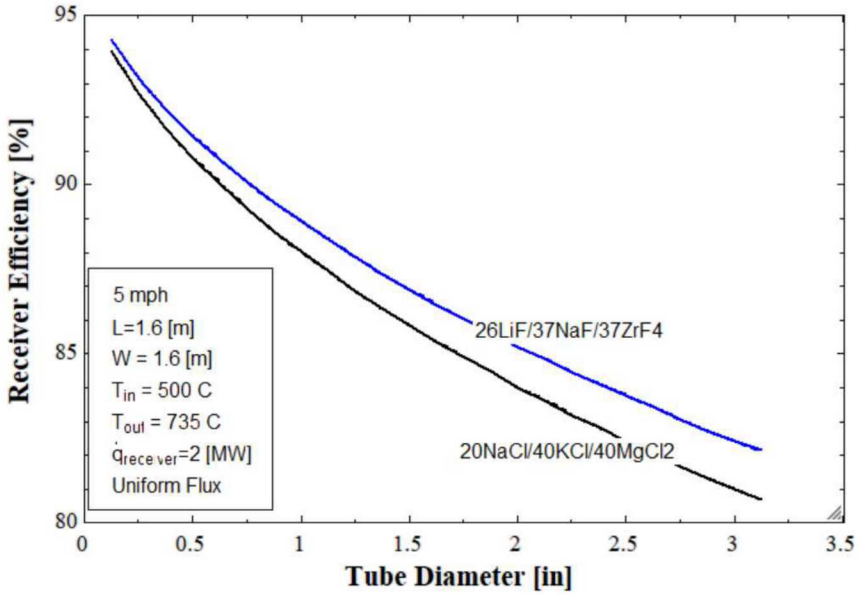

Figure 5. Calculated receiver efficiency as a function of receiver tube diameter and wind speed for a chloride and flouride molten salt, considering a 500 □ and 735 □ inlet and outlet temperature and a 2.56 m^2 aperature area.

System analysis for this investigation explored predicted dynamic head losses as a function of respective cold and hot pump flow rates. Here, system and ideal pump curves were calculated where recirculation was considered by a number of throttle valves with a determined C_v value. Preliminary pump designs for the cold and hot-leg pumps estimated the operating range for the two pumps to be between 1800 and 2400 RPM. The design shown in Fig. 1 has approximately 400 ft. and 433 ft. of 2.5 in. ID Sch. 80 piping for the hot and cold legs respectively. Calculations of flow head, along with initial pump designs estimated both hot and cold pump nominal flow rates to be as high as 110 GPM to meet requirements for both steady and transient (not considered here) operational modes. A generalized pump curve for 2400 RPM pump speed was calculated for a long-shafted pump based on an approximated dead-head of 99 ft and 332 ft, and a best efficiency point (BEP) head of 90 ft and 302 ft for the cold and hot pumps respectively. Recirculation control studies were performed where it was found that the cold recirculation mass fraction range was between 0.025 to 0.26 and the hot recirculation mass fraction was between 0.225 to 0.6, therefore the team set the respective minimum values to 0.025 and 0.225 respectively.

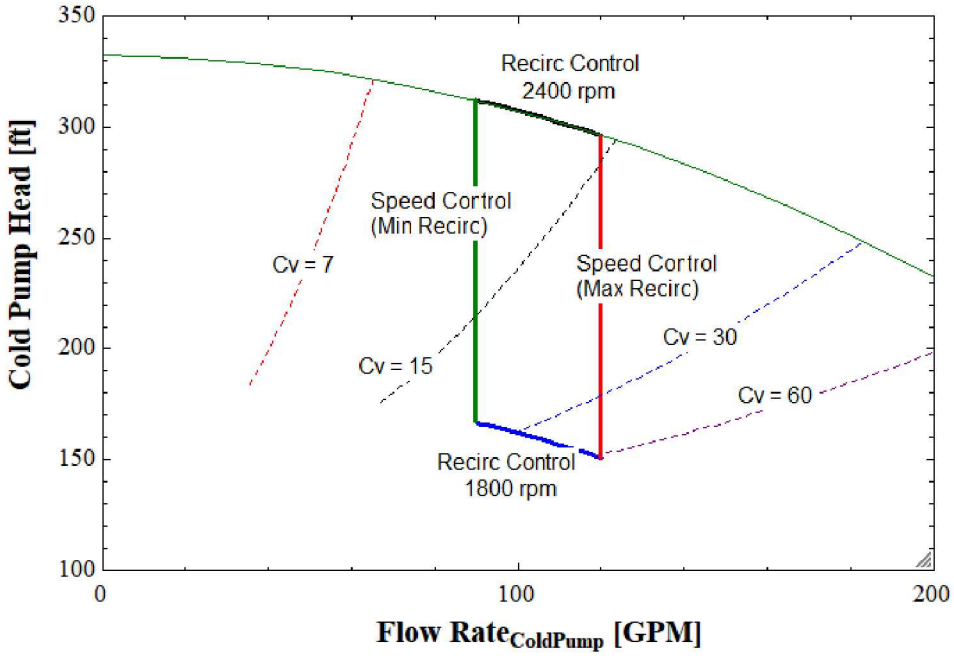

Figure 6. Ternary chloride molten salt system and pump curves for the cold pump.

As shown in Fig. 6 the cold pump operating envelope is bound by minimum and maximum speed control of the recirculating throttle valves as well as the 1800 and 2400 RPM pump operating points. For these operating points respective TDH values were determined to be respectively 181.6-165.9 ft. and 311.2-327 ft. for pump flow rates of 90-120 GPM. The results also suggest a reciculating throttle valve minimum C_v of 60 required to meet the operational envelope spanning the RPM range considered here.

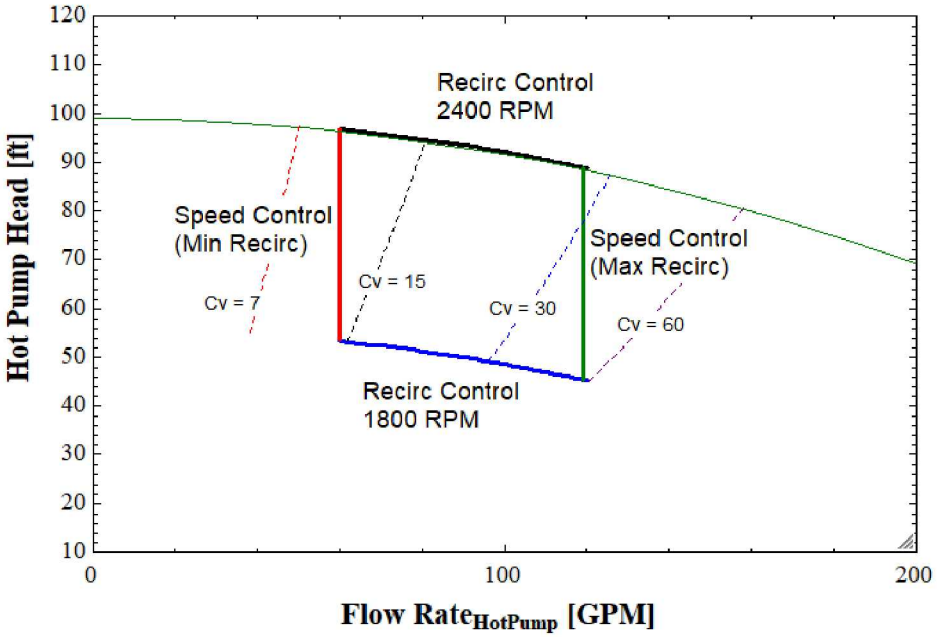

Figure 7. Ternary chloride molten salt system and pump curves for the hot pump.

For the hot pump, Fig. 7 results suggest TDH values between 49.65-57.73 ft. and 93.19-101.3 ft. for 1800 and 2400 RPM operational points. Similarly, a minimum Cv of 60 was also determined for the hot-side throttle recirculation valve for the operational envelope assessed here. Overall, for both throttle recirculation valves, the results suggest relatively high Cv values requiring minimal pressure drops necessitating pump operating points with minimal recirculation.

CONCLUSIONS

A system layout for a 2-MW_{th} chloride molten-salt test loop is presented, including a thermodynamic system model developed using EES to model operational states during various operational modes. Two different chloride salt chemistries were compared to each other with respect to required flux and efficiencies to achieve system design criteria including cold and hot tank temperatures of 500 □ and 720 □, as well as a 2.0 MW_{th} input power level and 1 MW_{th} PHX design. The model was developed with respect to uniform receiver flux spreading and steady operation, however future studies will include receiver flux distributions and transient operational modes. Results from this investigation suggest a non-linear variation with receiver tube diameter, where the ternary chloride salt required an average 11.1% lower receiver flux with a slightly lower calculated receiver efficiency when compared to the ternary fluoride salt. System performance was evaluated for the cold and hot pumps and respective recirculation throttling valves. The results suggest a minimum *C*v of 60 required for both cold and hot throttle recirculation valves for the operational pump speeds between 1800 and 2400 RPM.

REFERENCES

1. S.S.M. Tehrani, Y. Shoraka, K. Nithyanandam, and R.A. Taylor, (2018), Cyclic performance of cascaded and multi-layered solid-PCM shell-and-tube thermal energy storage systems: A case study of the 19.9 MW e Gemasolar CSP plant. Applied Energy, 228, pp.240-253.
2. R.I. Dunn, P.J. Hearps, and M.N. Wright, (2012), Molten-salt power towers: newly commercial concentrating solar storage. Proceedings of the IEEE, 100(2), pp.504-515.
3. M. Mehos, C. Turchi, J. Vidal, M. Wagner, Z. Ma, C.K. Ho, W. Kolb, C. Andraka, and A. Kruizenga, (2017), Concentrating Solar Power Gen3 Demonstration Roadmap, NREL/TP-5500-67464, NREL.
4. P.D. Myers Jr, and D.Y. Goswami, (2016), Thermal energy storage using chloride salts and their eutectics. Applied Thermal Engineering, 109, pp.889-900.
5. M.T. Islam, N. Huda, A.B. Abdullah and R. Saidur, (2018) A comprehensive review of state-of-the-art concentrating solar power (CSP) technologies: current status and research trends. Renewable and Sustainable Energy Reviews, 91, pp.987-1018.
6. J.C. Vidal and N. Klammer, (2019), Molten chloride technology pathway to meet the US DOE sunshot initiative with Gen3 CSP. In AIP Conference Proceedings, 2126, No. 1, AIP Publishing.
7. D.F. Williams, (2006), Assessment of candidate molten salt coolants for the NGNP/NHI heat-transfer loop, No. ORNL/TM-2006/69, Oak Ridge National Lab, Oak Ridge, TN, USA.